Near-Optimal Multi-Robot Motion Planning with Finite Sampling

Dror Dayan[1], Kiril Solovey[2], Marco Pavone[2], and Dan Halperin[1]

Abstract— **An underlying structure in several sampling-based methods for continuous multi-robot motion planning (MRMP) is the tensor roadmap (TR), which emerges from combining multiple PRM graphs constructed for the individual robots via a tensor product. We study the conditions under which the TR encodes a near-optimal solution for MRMP—satisfying these conditions implies near optimality for a variety of popular planners, including dRRT*, and the discrete methods M* and CBS when applied to the continuous domain. We develop the first finite-sample analysis of this kind, which specifies the number of samples, their deterministic distribution, and magnitude of the connection radii that should be used by each individual PRM graph, to guarantee near-optimality using the TR. This significantly improves upon a previous asymptotic analysis, wherein the number of samples tends to infinity, and supports guaranteed high-quality solutions in practice, within bounded running time. To achieve our new result, we first develop a sampling scheme, which we call the *staggered grid*, for finite-sample motion planning for individual robots, which requires significantly less samples than previous work. We then extend it to the much more involved MRMP setting which requires to account for interactions among multiple robots. Finally, we report on a few experiments that serve as a verification of our theoretical findings and raise interesting questions for further investigation.**

I. INTRODUCTION

Multi-robot (MR) systems are already playing a crucial role in manufacturing, warehouse automation, and natural resource monitoring, and in the future they will be employed in even broader domains from space exploration to search-and-rescue. One of the most basic ingredients necessary in all those applications are mechanisms for multi-robot motion planning (MRMP), which should quickly generate motion trajectories to move robots from their origins to destinations, while avoiding collisions with the environment and between robots. In many cases, it is desirable to develop MRMP approaches that provide strong guarantees of completeness and near-optimality, to ensure that a high-quality solution would be found (if one exists). To achieve this, methods for MRMP must accurately capture the continuous state space of individual robots and the intricate interactions between multiple robots. Those considerations make the task of designing efficient high-quality methods for MRMP tremendously challenging [1–4].

In this work we develop a general approach for near-optimal sampling-based motion planning using a finite number of samples, which is the first of its kind. Previous solutions guarantee path quality for the multi-robot case only asymptotically, namely, as the number of samples tends to infinity. In contrast, our new method explicitly prescribes finite samples sets, and by that supports guaranteed high-quality solutions in practice, within bounded running time.

Related work. A common approach to MRMP, which is often taken in the AI research community, is to consider a discretized version of the problem, termed multi-agent pathfinding (MAPF), wherein robots are assumed to move along vertices of a graph. A variety of methods were developed for MAPF, including integer-programming formulations [5], path-based search methods [6], and conflict-based search [7]. Those have been successfully applied to a variety of problems involving multiple robots—from warehouse management [8] to multi-drone package delivery [9]. Unfortunately, MAPF methods provide no solution quality guarantees with respect to the original continuous MRMP problem, since they usually employ a crude discretization of the robots' environment in the form of a regular lattice, where a cell size corresponds to a robot's bounding box.

Recent work extends conflict-based search to the continuous MRMP domain, by using PRM graphs to capture the individual robots' state space [10–12]. Nevertheless, no guidelines are provided as to how to construct those roadmaps (in terms of number of samples, their distribution, and connection radius) to guarantee completeness or optimality with respect to the original MRMP problem.

In a different line of work, computational geometry methods are employed to explicitly reason about the robots' continuous state space. Such methods are quite powerful, in that they guarantee polynomial runtime, completeness, and near-optimal solutions for different quality metrics [13–16]. However, those methods are typically restricted to disc-shaped robots operating within a planar domain, and they require special separation constraints, e.g., between the robots' initial and terminal positions, in order to work correctly, which limits their applicability in practice.

A promising direction, which aims to overcome the limitations of discrete and geometry-based approaches, are sampling-based (SB) planners. SB-planners were initially developed to the tackle the single-robot motion-planning problem for complex systems, by using random sampling of states to capture the structure of the robot's complex state space, which results in a discrete graph representation. Many of those algorithms, including the celebrated PRM [17, 18], and RRT [19, 20] algorithms are known to converge to a solution asymptotically with the number of samples drawn. Some SB-planners are also guaranteed to converge to the optimal solution as the number of samples tends to infinity [21–25].

Consequently, a variety of SB-MRMP approaches have emerged, from methods that aim to apply PRM-based solutions [26, 27], to techniques that sample local instances of the MAPF problem [28, 29]. A different method, termed

discrete RRT (`dRRT`) [30], carefully explores an implicitly-represented tensor roadmap (TR), which emerges from combining several `PRM` roadmaps constructed for the individual robots, to effectively solve instances of MRMP requiring tight coordination between multiple robots. A recent work further improves this approach with the `dRRT`* method [31], which is also shown to yield a near-optimal MRMP solution. To the best of our knowledge, this is the only scalable SB-MR planner with such a guarantee. Unfortunately, this result is asymptotic and does not specify guarantees for a finite number of samples.

Contribution. We develop a general framework for near-optimal SB-MRMP while using a finite number of samples. To this end, we study the structure of the TR which is an underlying ingredient in `dRRT`*, `MC-CBS` [11] (a continuous-space extension of `CBS`), and `M`* [6] (when applied to a continuous space). We develop conditions under which the TR encodes a near-optimal solution to MRMP—if those conditions hold, it implies that the aforementioned planners are guaranteed to be near-optimal as well. In particular, we prescribe a recipe for constructing individual-robot `PRM` graphs, in terms of number of samples, their deterministic distribution, and connection radius, so that the resulting TR encodes a near-optimal solution for MRMP.

To achieve this we refine the asymptotic analysis that we developed in [31] (in the context of the `dRRT`* algorithm) to the finite-sample regime. The latter requires a much more careful study of the different ingredients of the problem, including the clearance parameter between robots and obstacles, and the approximation factor, which were previously assumed to be infinitesimally small. A key component in our result is a new sampling scheme that we develop, which we call the *staggered grid*, for finite-sample motion planning for individual robots. This sampling scheme requires significantly less samples than our previous work [32], to achieve near-optimality for the single-robot case.

The organization of this paper is as follows. In Section II we describe the single-robot problem, introduce the staggered grid, and study the theoretical properties of `PRM` using this sampling scheme. In Section III we describe our central contribution, namely the extension of this theoretical result to the multi-robot setting. We provide experimental results in Section IV, and conclude with an outline of future work in Section V. An extended version of this paper provides additional information and missing proofs [33].

II. IMPROVED SAMPLING DISTRIBUTIONS FOR A SINGLE ROBOT

We present our contribution regarding improved sampling distributions for probabilistic roadmaps (`PRM`) for the *single-robot* case. First, we introduce basic ingredients of the problem, then review the concept of `PRM`, and introduce our staggered-grid sampling. We conclude with our main theoretical result for the single-robot case, pertaining to the quality of solutions obtained using `PRM` with staggered-grid sampling.

A. Basics of single-robot motion planning

Let $\mathcal{C}$ denote the configuration space of the robot, which we assume here to be $[0,1]^d$, where d is the dimension.

The free space, denoted by $\mathcal{C}^f \subset \mathcal{C}$, represents the set of all collision-free configurations. A motion planning problem is a tuple $\mathcal{M} := (\mathcal{C}^f, x^s, x^g)$, where $\mathcal{C}^f$ is the free space, and $x^s, x^g \in \mathcal{C}^f$ are the start and goal configurations, respectively. A solution of $\mathcal{M}$ is a continuous collision-free trajectory $\sigma : [0,1] \to \mathcal{C}^f$ that begins in $\sigma(0) = x^s$ and ends at $\sigma(1) = x^g$. We measure the quality of a trajectory σ by its length, which is denoted by $\|\sigma\|$.

A crucial property of trajectories in sampling-based planning is the notion of clearance. A trajectory σ has δ-clearance if $\bigcup_{0 \leq t \leq 1} B_\delta(\sigma_i(t)) \subseteq \mathcal{C}^f$, for $B_\delta(\sigma_i(t))$ being the d-dimensional closed Euclidean ball with radius δ centered at $\sigma_i(t)$. We say that $\mathcal{M}$ is δ-clear if there exists a trajectory σ with clearance δ that solves $\mathcal{M}$.

B. Probabilistic roadmaps and sample sets

We provide a formal definition of the Probabilistic Roadmap (`PRM`) method [17], which constructs a discrete graph that captures the connectivity of $\mathcal{C}^f$ via sampling. `PRM` plays a critical role in various sampling-based planners (see, e.g., [32, 34]). `PRM` is also instrumental to our result both on single-robot motion-planning in this section and on multi-robot motion-planning in Section III.

For a given motion-planning problem $\mathcal{M} = (\mathcal{C}^f, x^s, x^g)$, a sample (point) set $\mathcal{X} \subset \mathcal{C}^f$, and a connection radius $r > 0$, `PRM` generates a graph denoted by $G_{\mathcal{M}}(\mathcal{X}, r) = (V, E)$. The vertex set V consists of all the collision-free configurations in $\mathcal{X} \cup \{x^s, x^g\}$. The set of (undirected) edges, E, consists of all vertex pairs $v, u \in V$ such that the Euclidean distance between them is at most r, and the straight-line segment between them is collision-free. Formally, we define $V := (\mathcal{X} \cup \{x^s, x^g\}) \cap \mathcal{C}^f$ and

$$E := \left\{ \{v, u\} \in V \times V : \|v - u\| \leq r, \text{CH}(\{v, u\}) \subset \mathcal{C}^f \right\},$$

where CH denotes the convex hull of a point set.

To measure the quality of a sample set $\mathcal{X}$ and a connection radius r we use the following definition [32].

Definition 1 (Single-robot (ε, δ)-completeness)**.** Given a sample set $\mathcal{X}$ and connection radius r, we say that $(\mathcal{X}, r)$ is (ε, δ)-complete for some stretch $\varepsilon > 0$ and clearance parameter $\delta > 0$ if for every δ-clear $\mathcal{M} = (\mathcal{C}^f, x^s, x^g)$ it holds that

$$d_{G_{\mathcal{M}}(\mathcal{X}, r)}(x_i^s, x_i^g) \leq (1 + \varepsilon)\text{OPT}_\delta,$$

where $d_{G_{\mathcal{M}}(\mathcal{X}, r)}(x^s, x^g)$ denotes the length of the shortest trajectory from x^s to x^g in the graph $G_{\mathcal{M}}(\mathcal{X}, r)$, and OPT_δ is the length of the shortest δ-clear solution to $\mathcal{M}$.

C. Efficient sampling via a staggered grid

In preparation for our main result in this section we introduce a new sampling scheme termed a *staggered grid*, which we denote by $\mathcal{X}_{\beta,\gamma}$, and study its implications with respect to (ε, δ)-completeness of `PRM`. Refer to Figure 1 for an illustration. An important property of this staggered grid, which we prove in the extended version [33], is that by placing β-radius hyperspheres centered at the points $\mathcal{X}_{\beta,\gamma}$ we obtain a coverage of the robot's configuration space. Moreover, the size of the set $\mathcal{X}_{\beta,\gamma}$ is smaller than previously obtained sets with similar coverage properties [32].

Definition 2 (Staggered grid)**.** For given $\beta > 0, \gamma > 0$ the staggered grid $\mathcal{X}_{\beta,\gamma}$ is a union of two point sets $\mathcal{X}_{\beta,\gamma}^1, \mathcal{X}_{\beta,\gamma}^2$

in $[0,1]^d$, where

$$\mathcal{X}_{\beta,\gamma}^1 = \left\{ (p_1, p_2, ..., p_d) : p_i = \gamma + (2k-1)w, \right.$$

$$\left. 1 \leq k \leq \left\lceil \frac{1-2\gamma}{2w} \right\rceil, 1 \leq i \leq d \right\}$$

$$\mathcal{X}_{\beta,\gamma}^2 = \left\{ (p_1, p_2, ..., p_d) : p_i = \gamma + (2k), w \right.$$

$$\left. 0 \leq k \leq \left\lceil \frac{1-2\gamma}{2w} \right\rceil, 1 \leq i \leq d \right\},$$

where $w = \frac{\beta\sqrt{2}}{\sqrt{d}}$.

Notice that both $\mathcal{X}_{\beta,\gamma}^1$ and $\mathcal{X}_{\beta,\gamma}^2$ are square grids of side length $2w$, and the total number of points in the construction is $\left(\left\lceil \frac{(1-2\gamma)\sqrt{d}}{\sqrt{8}\beta} \right\rceil \right)^d + \left(\left\lceil \frac{(1-2\gamma)\sqrt{d}}{\sqrt{8}\beta} \right\rceil + 1 \right)^d$.

Next we make the connection between the staggered grid and a PRM graph that is (ε, δ)-complete. Namely, we will show that given ε and δ, there is a sample set and radius $(\mathcal{X}_{\beta,\gamma}, r)$ that are (ε, δ)-complete, where β depends on both ε and δ, γ is equal to δ, and r depends on both ε and δ.

Theorem 1 (Sufficient conditions for (ε, δ)-completeness). Fix a stretch parameter $\varepsilon > 0$ and clearance $\delta > 0$. For a sampling distribution $\mathcal{X} = \mathcal{X}_{\alpha\delta,\delta}$, where $\alpha = \frac{\varepsilon}{\sqrt{1+\varepsilon^2}}$, and radius $r = 2(\alpha + \sqrt{1-\alpha^2})\delta$, it follows that $(\mathcal{X}, r)$ is (ε, δ)-complete.

D. Proof of Theorem 1

In this section we provide a proof of Theorem 1. First, we introduce the concept of β-cover [35]. Informally, a β-cover of a domain is a set $\mathcal{X}$ of points such that no point of the domain is too far from some point in $\mathcal{X}$ (defined formally below). Next we show that the staggered grid $\mathcal{X}_{\beta,\delta}$ is a β-cover of $[\delta, 1-\delta]^d$. Then we exploit this property in the proof for Theorem 1.

Definition 3. For a given $\beta > 0$, a set $\mathcal{X} \subset \mathbb{R}^d$ is a β-cover[1] for a set $A \subset \mathbb{R}^d$ if for every $a \in A$, there exists $s \in \mathcal{X}$ such that $\|a - s\| \leq \beta$

First, we prove that $\mathcal{X}_{\beta,\gamma}$ forms a β-cover over $\mathcal{A}_\gamma$.

---

[1] The common naming for this is ε-cover. We use the letter β to avoid confusion with the stretch factor which is called ε in this paper. We also note that the term β-cover is a more accurate substitution for the term "β-net", which we used in our previous work [32].
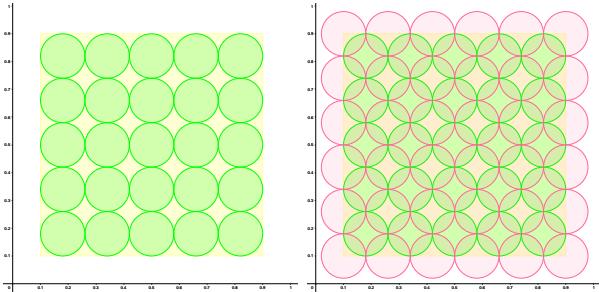

Fig. 1: Illustration of Definition 2 in two dimensions, for $\beta = 0.08$, $\gamma = 0.1$. On the left we visualize the first layer $\mathcal{X}_{\beta,\gamma}^1$ of the staggered grid (denoted by green balls). On the right we add the second layer $\mathcal{X}_{\beta,\gamma}^2$ (denoted by red balls).

Lemma 2. Let $\beta > 0, \gamma > 0$ and define $A_\gamma = [\gamma, 1 - \gamma]^d$. Then the staggered grid $\mathcal{X}_{\beta,\gamma}$ is a β-cover for A_γ.

Proof. Recall that the width w of a cell in each of the two grids that form the staggered grid $\mathcal{X}_{\beta,\gamma}$ is $\beta\sqrt{2}/\sqrt{d}$. We divide the d-dimensional $(1 - 2\gamma)$-hypercube, A_γ by hyperplanes as follows. For each coordinate x_i we define the hyperplanes $x_i = \gamma + 2kw$, for $k \in \{0, 1, \ldots, \lceil \frac{1-2\gamma}{2w} \rceil\}$. Jointly, those hyperplanes induce a partition of A_δ into a set of hypercubes H: each hypercube $h \in H$ is of edge length $2w$, its center is a point from $\mathcal{X}_{\beta,\gamma}^1$, and its vertices are points from $\mathcal{X}_{\beta,\gamma}^2$. See Figure 2 for an illustration in $\mathbb{R}^2$.
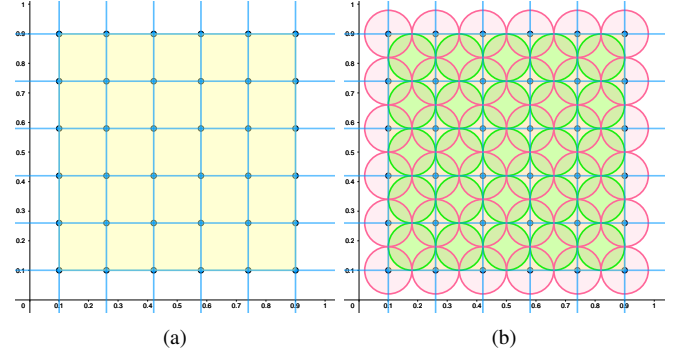

Fig. 2: Illustration of the hyperplanes partition for Lemma 2 in two dimensions, for $\gamma = 0.1$, $\beta = 0.08$ ($\Rightarrow w = 0.08$). In both sub-figures the yellow cube represents $[\gamma, 1 - \gamma]^d$, and the blue lines are the hyperplanes orthogonal to x_i. In (a) we demonstrate how the cube is split into smaller $2w$-cubes. In (b) we demonstrate that these $2w$-cubes are covered with β-balls (for $\beta = 0.08$). The green balls are β-balls centered at points of $\mathcal{X}_{\beta,\gamma}^1$, while the red balls are β-balls centered at points of $\mathcal{X}_{\beta,\gamma}^2$.

We now prove that each $h \in H$ induced by our hyperplanes is fully covered using the β-balls centered at its vertices and at its center. For a given $h \in H$, let S_h be the set of points comprised of the vertices of h and the center point of h (i.e., $|S_h| = 2^d + 1$). We show that S_h is a β-cover for h.

Let $s \in S_h$ be the the center point of h. Without loss of generality, assume that s is at the origin. Let $B_\beta(s)$ be the β-ball centered at s. Let $p = (p_1, .., p_d)$ be a d-dimensional point such that $p \in h$ and $p \notin B_\beta(s)$. We further assume that $\forall i \in [1..d], 0 \leq p_i \leq w$; all the other cases can be handled symmetrically. Thus, since $p \notin B_\beta(s)$ we have that $\|s - p\| > \beta$, which implies that $\beta^2 < \sum_{i=1}^d p_i^2$.

Next, recall that $s_w := (w, ..., w) \in S$ since the hypercubes edge length is $2w$. We upper bound the distance of p from s_w in the following manner:

$$\|s_w - p\|^2 = \sum_{i=1}^d (w - p_i)^2 = \sum_{i=1}^d (w^2 - 2wp_i + p_i^2)$$

$$\leq \sum_{i=1}^d (w^2 - 2p_i^2 + p_i^2)$$

$$= \sum_{i=1}^d w^2 - \sum_{i=1}^d p_i^2 < \sum_{i=1}^d w^2 - \beta^2,$$

where the first inequality follows from the fact that $p_i \leq w$, and the second inequality follows from $\beta^2 < \sum_{i=1}^d p_i^2$.

Finally, by subsisting $w = \beta\sqrt{2}/\sqrt{d}$, we obtain

$$\|s_w - p\|^2 < \sum_{i=1}^{d} \frac{2\beta^2}{d} - \beta^2 = \beta^2,$$

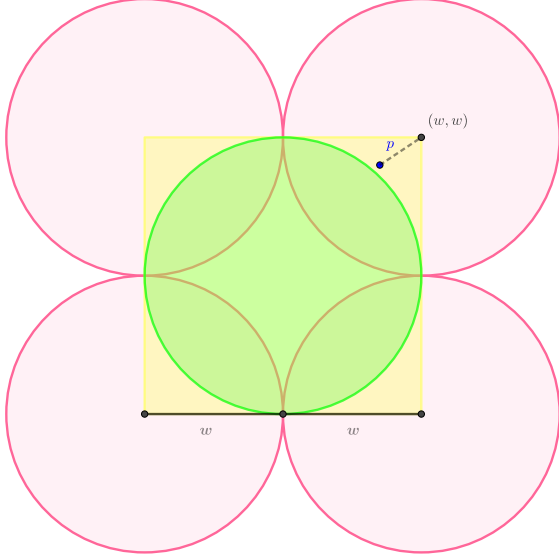which implies that p is covered by the β-ball centered at s_w.

Fig. 3: Illustration of the covering of a $2w$-hypercube of Lemma 2 in two dimensions, for $w = 1$. The point p is the point tested in the lemma. The red balls are β-balls centered on the cube vertices. The green ball is the β-ball centered in the cubes center called $B_\beta(s)$. The dashed line represents the distance between p and (w, w). We note that in higher dimensions the red balls would overlap as w becomes smaller in relation to β.

We have proven that $\mathcal{X}_{\beta,\gamma}$ provides a β-cover for each $h \in H$, which also guarantees that $\mathcal{X}_{\beta,\gamma}$ is a β-cover for the larger hypercube $[\gamma, 1-\gamma]^d$. Thus we conclude that $\mathcal{X}_{\beta,\gamma}$ is a β-cover for A_γ. $\square$

Next, we exploit the above property in showing that by setting correctly the values of β, γ and r with respect to ε, δ, we obtain a good approximation of any collision-free trajectory, which implies that $(\mathcal{X}_{\beta,\gamma}, r)$ is (ε, δ)-complete. To do so, we prove the following theorem, which is an extended version of [32, Theorem 2]. This theorem, will also be instrumental in extending the theory we develop for the single-robot case, to the multi-robot setting. In order to state the theorem, we introduce additional notation regarding a sequence of points along a given trajectory of certain spacing.

Definition 4. Let σ be a collision-free trajectory, and let $\rho > 0$ be a step size such that $\|\sigma(0) - \sigma(1)\| \geq \rho$. Then the order timing set $T_\sigma^\rho = (\tau_0, \tau_1, \ldots, \tau_\ell)$, where $\tau_0 < \tau_1 \ldots < \tau_\ell$, is defined in the following manner for some $\ell \in \mathbb{N}_{>0}$: $\tau_0 = 0, \tau_\ell = 1$, for all $1 \leq i \leq \ell-1$, $\|\sigma(\tau_i) - \sigma(\tau_{i-1})\| = \rho$, and $\|\sigma(\tau_\ell) - \sigma(\tau_{\ell-1})\| \leq \rho$.

Lemma 3. For given $\beta, \gamma, \rho > 0$, such that $\beta^2 + (\rho/2)^2 \leq \gamma^2$, let σ be a γ-clear solution for $\mathcal{M} = (\mathcal{C}^f, x^s, x^g)$, and let $T_\sigma^\rho = (\tau_0, \tau_1, \ldots, \tau_\ell)$ as in Definition 4. Then there exists a point set $Z_\sigma^\rho = (z_0, \ldots, z_\ell)$, where $z_i \in \mathcal{X}_{\beta,\gamma} \cup \{x^s, x^g\}$ for all $0 \leq i \leq \ell$, such that the following holds:

(i) $\|z_i - \sigma(\tau_i)\| \leq \beta$, for all $0 \leq i \leq \ell$;

(ii) $\|z - \sigma(\tau_{i-1})\| \leq \beta + \rho$, for all $1 \leq i \leq \ell$, $z \in$ CH(z_{i-1}, z_i);

(iii) $\|z - \sigma(\tau_i)\| \leq \beta + \rho$, for all $1 \leq i \leq \ell$, $z \in$ CH(z_{i-1}, z_i);

(iv) $\|z_i - z_{i-1}\| \leq 2\beta + \rho$, for all $1 \leq i \leq \ell$;

(v) CH(z_{i-1}, z_i) is collision free, for all $1 \leq i \leq \ell$. That is CH$(z_{i-1}, z_i) \subset \mathcal{C}^f$, for all $1 \leq i \leq \ell$;

(vi) $\sum_{1 \leq i \leq \ell} \|z_i - z_{i-1}\| \leq \left(1 + \frac{2\beta}{\rho}\right) \|\sigma\|$.

Proof. Define $A_\gamma = [\gamma, 1-\gamma]^d$. Note that since σ is γ-clear then $\sigma(t) \in A_\gamma$ for all $0 \leq t \leq 1$ (and in particular for all $\tau_i \in T_\sigma^\rho$). Next, we address the individual component of the theorem.

Property (i): This follows directly from Lemma 2 as $\mathcal{X}_{\beta,\gamma}$ is a β-cover for A_γ and $\sigma(\tau_i) \in A_\gamma$.

Properties (ii) and (iii): First, we upper bound the expression $\|z_i - \sigma(\tau_{i-1})\|$ (the proof for property (iii) is symmetric). By definition of T_σ^ρ note that $\|\sigma(\tau_i) - \sigma(\tau_{i-1})\| = \rho$. Thus, using property (i), we have $\|z_i - \sigma(\tau_i)\| \leq \beta$. Using the triangle inequality it follows that,

$$\|z_i - \sigma(\tau_{i-1})\| \leq \|z_i - \sigma(\tau_i)\| + \|\sigma(\tau_i) - \sigma(\tau_{i-1})\| \leq \beta + \rho.$$

Let $z \in$ CH(z_{i-1}, z_i), that is $z = \lambda z_{i-1} + (1 - \lambda)z_i$ for some λ such that $0 \leq \lambda \leq 1$. Thus,

$$\|z - \sigma(\tau_{i-1})\|$$
$$= \|\lambda z_{i-1} + (1-\lambda)z_i - \sigma(\tau_{i-1})\|$$
$$= \|\lambda z_{i-1} - \lambda\sigma(\tau_{i-1}) + (1-\lambda)z_i - (1-\lambda)\sigma(\tau_{i-1})\|$$
$$\leq \|\lambda z_{i-1} - \lambda\sigma(\tau_{i-1})\| + \|(1-\lambda)z_i - (1-\lambda)\sigma(\tau_{i-1})\|$$
$$= \lambda\|z_{i-1} - \sigma(\tau_{i-1})\| + (1-\lambda)\|z_i - \sigma(\tau_{i-1})\|,$$

where the triangle inequality was used in the second-to-last transition. Due to property (i) and the fact that $\|z_i - \sigma(\tau_{i-1})\| \leq \beta + \rho$ it follows that

$$\|z - \sigma(\tau_{i-1})\| \leq \lambda\beta + (1-\lambda)(\beta+\rho) = \beta + (1-\lambda)\rho \leq \beta + \rho.$$

Property (iv): This follows from properties (i) and (ii), and triangle inequality:

$$\|z_i - z_{i-1}\| \leq \|z_i - \sigma(\tau_{i-1})\| + \|\sigma(\tau_{i-1}) - z_{i-1}\| \leq 2\beta + \rho.$$

Property (v): Fix $1 \leq i \leq \ell$. For any $\eta \in [0, 1]$ define $u_\eta = \eta z_{i-1} + (1-\eta)z_i$. To prove that property (v) holds we will show that $u_\eta \in \mathcal{C}^f$ for every $\eta \in [0, 1]$.

Fix $\eta \in [0, 1]$. Since $\sigma(\tau_{i-1}), \sigma(\tau_i)$ are points on a γ-clear path, the γ-balls $B_\gamma(\sigma(\tau_{i-1})), B_\gamma(\sigma(\tau_i))$ are collision-free. Thus it is sufficient to prove that $u_\eta \in B_\gamma(\sigma(\tau_{i-1})) \cup B_\gamma(\sigma(\tau_i))$. Next v_η be the closest point to u_η on the straight line between $\sigma(\tau_{i-1})$ and $\sigma(\tau_i)$. That is, $v_\eta = \arg\min_{v \in \text{CH}(\{\sigma(\tau_{i-1}), \sigma(\tau_i)\})} \|u_\eta - v\|$.

We also define $v'_\eta := \eta\sigma(\tau_{i-1}) + (1-\eta)\sigma(\tau_i)$, and prove that $\|u_\eta - v'_\eta\| \leq \beta$. This implies that $\|u_\eta - v_\eta\| \leq \beta$ as v_η is at least as close as v'_η to u_η. Indeed, using property (i) and the triangle inequality we have

$$\|u_\eta - v'_\eta\|$$
$$\leq \|\eta z_{i-1} + (1-\eta)z_i - (\eta\sigma(\tau_{i-1}) + (1-\eta)\sigma(\tau_i))\|$$
$$\leq \eta\|z_{i-1} - \sigma(\tau_{i-1})\| + (1-\eta)\|z_i - \sigma(\tau_i)\| = \beta.$$

Building upon this result, we consider several cases with respect to the position of v_η. If v_η is one of the endpoints, that is $v_\eta = \sigma(\tau_{i-1})$ or $v_\eta = \sigma(\tau_i)$, we have that u_η is in a β-ball around this point. Since $\beta^2 + (\rho/2)^2 \leq \gamma^2$, and

all are positive, we know that $\beta \leq \gamma$. Thus if v_η is one of the endpoints we are done as $u_\eta \in B_\beta(\sigma(\tau_{i-1}))$ or $u_\eta \in B_\beta(\sigma(\tau_i))$.

Assuming v_η is not one of the endpoints we can write $v_\eta = \eta^*\sigma(\tau_{i-1}) + (1 - \eta^*)\sigma(\tau_i)$ where

$$\eta^* = \arg\min_{\lambda \in (0,1)} \|u_\eta - \lambda\sigma(\tau_{i-1}) + (1 - \lambda)\sigma(\tau_i)\|.$$

As a consequence of the first order optimality conditions,

$$< \sigma(\tau_i) - \sigma(\tau_{i-1}), u_\eta - v_\eta >= 0$$

Since $\{\sigma(\tau_{i-1}), \sigma(\tau_i), v_\eta\}$ are collinear we get that,

$$< v_\eta - \sigma(\tau_{i-1}), u_\eta - v_\eta >= \qquad (1)$$
$$< v_\eta - \sigma(\tau_i), u_\eta - v_\eta >= 0 \qquad (2)$$
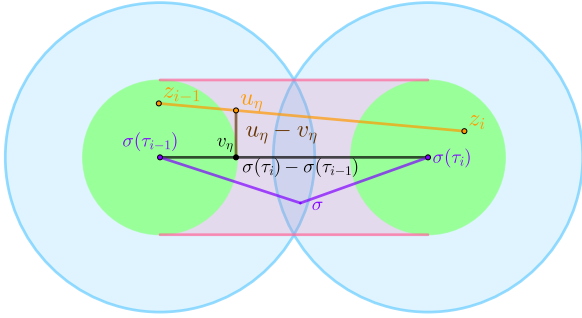

Fig. 4: Illustration for the proof of Lemma 3. The purple curve represents the trajectory σ. The green balls are the β-balls around $\sigma(\tau_{i-1})$ and $\sigma(\tau_i)$. This balls with the red zone are the space is which CH$(\{z_{i-1}, z_i\})$ is found, that is to say this union is required to be a collision-free space. This is demonstrated by the orange line between z_{i-1} and z_i which is their convex hull. The blue balls are collision-free γ-balls around $\sigma(\tau_{i-1})$ and $\sigma(\tau_i)$. The black line is CH$(\{\sigma(\tau_{i-1}), \sigma(\tau_i)\})$. Note that the line between u_η and v_η (brown line) is perpendicular to the line between $\sigma(\tau_{i-1})$ and $\sigma(\tau_i)$, these correspond to $u_\eta - v_\eta$ and $\sigma(\tau_i) - \sigma(\tau_{i-1})$ respectively. **the last part of the sentence is not clear. Can you elaborate?.**

We now consider two separate cases with respect to η^*. First assume $\eta^* \in (0, 1/2]$. Using Equation (2) and property (i), it follows that

$$\|u_\eta - \sigma(\tau_i)\|^2 = \|(u_\eta - v_\eta) + (v_\eta - \sigma(\tau_i))\|^2$$
$$= \|u_\eta - v_\eta\|^2 + \|v_\eta - \sigma(\tau_i)\|^2$$
$$\leq \beta^2 + \|\eta^*\sigma(\tau_{i-1}) + (1 - \eta^*)\sigma(\tau_i) - \sigma(\tau_i)\|^2$$
$$= \beta^2 + (\eta^*)^2 \|\sigma(\tau_{i-1}) - \sigma(\tau_i)\|^2$$
$$= \beta^2 + (\eta^*)^2 \rho^2 \leq \beta^2 + (1/2)^2 \rho^2,$$

where the last inequality follows from $\eta^* \leq 1/2$. Finally by plugging-in $\beta^2 + (\rho/2)^2 \leq \gamma^2$ we get $\|u_\eta - \sigma(\tau_i)\|^2 \leq \gamma^2$, which implies that $u_\eta \in B_\gamma(\sigma(\tau_i))$.

Due to symmetry, we can show that for $\eta^* \in (1/2, 1)$, it follows that $\|u_\eta - \sigma(\tau_{i-1})\|^2 \leq \gamma^2$, which again im-
$\longrightarrow$ plies $u_\eta \in B_\gamma(\sigma(\tau_{i-1}))$.**(DROR SAYS: In Matt's paper he fully showed it, shouldn't we do the same?)** To conclude, we showed that for all $\eta \in [0, 1]$ it holds that $u_\eta \in B_\gamma(\sigma(\tau_{i-1})) \cup B_\gamma(\sigma(\tau_i))$, which implies that CH$(z_{i-1}, z_i) \subset \mathcal{C}^f$.

Property (vi) Due to property (iv) we have that, $\|z_i - z_{i-1}\| \leq 2\beta + \rho$ for all $1 \leq i \leq \ell$. Since the staring point and end point for both σ and our trajectory are identical, we know that $z_0 = \sigma(0), z_1 = \sigma(1)$. This yields that only for the

first and last segment of movement we have $\|z_i - z_{i-1}\| \leq \beta + \|\sigma(\tau_i) - \sigma(\tau_{i-1})\|$. Using this we get,

$$\sum_{1 \leq i \leq \ell} \|z_i - z_{i-1}\|$$
$$= \|z_1 - z_0\| + \sum_{2 \leq i \leq \ell - 1} \|z_i - z_{i-1}\| + \|z_\ell - z_{\ell-1}\|$$
$$\leq \beta + \rho + \sum_{2 \leq i \leq \ell - 1} (2\beta + \rho) + \beta + \|\sigma(\tau_\ell) - \sigma(\tau_{\ell-1})\|$$
$$= \beta + \rho + (\ell - 2) \cdot (2\beta + \rho) + \beta + \|\sigma(\tau_\ell) - \sigma(\tau_{\ell-1})\|$$
$$= (2\beta + \rho) + (\ell - 2) \cdot (2\beta + \rho) + \|\sigma(\tau_\ell) - \sigma(\tau_{\ell-1})\|$$
$$= (\ell - 1) \cdot (2\beta + \rho) + \|\sigma(\tau_\ell) - \sigma(\tau_{\ell-1})\|$$

Additionally, due to $\|\sigma(\tau_i) - \sigma(\tau_{i-1})\| = \rho$ for all $1 \leq i \leq \ell - 1$, we have that $\|\sigma\| \geq (\ell - 1) \cdot \rho + \|\sigma(\tau_\ell) - \sigma(\tau_{\ell-1})\|$. Thus,

$$\frac{\sum_{1 \leq i \leq \ell} \|z_i - z_{i-1}\|}{\|\sigma\|}$$
$$\leq \frac{(\ell - 1) \cdot (2\beta + \rho) + \|\sigma(\tau_\ell) - \sigma(\tau_{\ell-1})\|}{(\ell - 1) \cdot \rho + \|\sigma(\tau_\ell) - \sigma(\tau_{\ell-1})\|}$$
$$\leq \frac{(2\beta + \rho)((\ell - 1) + \|\sigma(\tau_\ell) - \sigma(\tau_{\ell-1})\|/(2\beta + \rho))}{\rho((\ell - 1) + \|\sigma(\tau_\ell) - \sigma(\tau_{\ell-1})\|/\rho)}$$
$$= \frac{(2\beta + \rho)}{\rho} \cdot \frac{(\ell - 1) + \|\sigma(\tau_\ell) - \sigma(\tau_{\ell-1})\|/(2\beta + \rho)}{(\ell - 1) + \|\sigma(\tau_\ell) - \sigma(\tau_{\ell-1})\|/\rho}$$
$$\leq \frac{(2\beta + \rho)}{\rho} \cdot 1 = 1 + \frac{2\beta}{\rho}$$

Thus concluding this proof. $\square$

It remains to prove Theorem 1. To use Lemma 3, we set $\gamma = \delta, \beta = \alpha\delta, \rho = 2\sqrt{1 - \alpha^2}\delta$, and $r = 2(\alpha + \sqrt{1 - \alpha^2})\delta$, for $\alpha = \varepsilon/\sqrt{1 + \varepsilon^2}$, so that the condition $\beta^2 + (\rho/2)^2 \leq \gamma^2$ holds.

By setting $r = 2\beta + \rho = 2(\alpha + \sqrt{1 - \alpha^2})\delta$, it follows from Lemma 2 (iv) that for all $1 \leq i \leq \ell$ the PRM edge connecting z_i and z_{i-1} is considered in the PRM construction. Additionally, since $\frac{2\beta}{\rho} = \varepsilon$, it holds that $\|\hat{\sigma}\| \leq (1 + \varepsilon) \|\sigma\|$ where $\hat{\sigma}$ denotes the piece-wise linear trajectory induced by Z_σ^ρ, which concludes the proof.
    (DROR SAYS: From here.) $\longleftarrow$

E. Comparison between the staggered grid and previous work

We compare the minimal sample size required to guarantee (ε, δ)-completeness for the same single-robot setting, between the previous approach [32], and the staggered grid as proposed here. We denote by $\mathcal{X}_{\text{prev}}$ the size of the minimal sample set needed using the bound from [32], namely

$$\mathcal{X}_{\text{prev}} = \sqrt{\pi d} \left(\sqrt{\frac{2d}{\pi e}} \cdot \frac{1 - (2 - \alpha)\delta}{\alpha\delta} \right)^d.$$

We denote by $\mathcal{X}_{\text{curr}} = |\mathcal{X}_{\alpha\delta,\delta}|$ the size of the minimal sample set needed using the bound for the staggered grid, as stated in Theorem 1, namely

$$X_{\text{curr}} = \left(\left\lceil \frac{(1 - 2\delta)\sqrt{d}}{\sqrt{8}\alpha\delta} \right\rceil \right)^d + \left(\left\lceil \frac{(1 - 2\delta)\sqrt{d}}{\sqrt{8}\alpha\delta} \right\rceil + 1 \right)^d.$$

We compare the quantities $\mathcal{X}_{\text{prev}}$ and $\mathcal{X}_{\text{curr}}$ for small values of ε and δ (we mention that the radius derived in [32] is

equal to the one we are using here). We look at the ratio $\frac{\mathcal{X}_{\text{prev}}}{\mathcal{X}_{\text{curr}}}$ asymptotically as ε and δ tend to zero[2] (Eq. 3), as well as numerically for low-dimensional configuration spaces (Table ??).

$$
\begin{aligned}
\frac{\mathcal{X}_{\text{prev}}}{\mathcal{X}_{\text{curr}}} &= \frac{\sqrt{\pi d}\left(\sqrt{\frac{2d}{\pi e}} \cdot \frac{1-(2-\alpha)\delta}{\alpha\delta}\right)^d}{\left(\frac{(1-2\delta)\sqrt{d}}{\sqrt{8}\alpha\delta}\right)^d + \left(\frac{(1-2\delta)\sqrt{d}}{\sqrt{8}\alpha\delta}+1\right)^d} \\
&= \frac{\sqrt{\pi d}\left(\sqrt{\frac{2d}{\pi e}} \cdot \frac{1-2\delta+\alpha\delta}{\alpha\delta}\right)^d}{\left(\frac{(1-2\delta)\sqrt{d}}{\sqrt{8}\alpha\delta}\right)^d + \left(\frac{(1-2\delta)\sqrt{d}}{\sqrt{8}\alpha\delta}+1\right)^d} \quad (3) \\
&\overset{(a)}{\approx} \frac{\sqrt{\pi d}\left(\sqrt{\frac{2d}{\pi e}} \cdot \frac{1-2\delta}{\alpha\delta}\right)^d}{2\left(\frac{(1-2\delta)\sqrt{d}}{\sqrt{8}\alpha\delta}\right)^d} \\
&= \frac{\sqrt{\pi d}}{2}\left(\sqrt{\frac{16}{\pi e}}\right)^d \approx \frac{\sqrt{\pi d}}{2} 1.3687^d,
\end{aligned}
$$

where (a) is due to ignoring the $\alpha\delta$ from the numerator of the numerator, and also ignoring the $+1$ from the denominator, both influences tend to 0 as δ or ε tend to 0. Thus we improved the previous bound by an exponential factor in $\longrightarrow$ d. (**DROR SAYS**: Note to self, if $d > 5$, I can make both top and bottom look like $(a+1)^d$, and I believe that when $a > b$, $((a+1)/(b+1))^d \leq (a/b)^d$. This means, I can make the bound true for all ε, δ.)

We provide a comparison of the concrete number of samples for a few values of δ and ε in low dimensions in Table ??. As one can see, in all the reported cases, the staggered grid is between 6- and 16-fold more economical $\longrightarrow$ than the sample set of [32, Theorem 2]. (**DROR SAYS**: Add table, note that in the ICRA version we said we will add both comparison to the prev and to the lower bound.)

III. NEAR-OPTIMAL TENSOR ROADMAPS FOR MRMP

We present our central contribution: we extend our results from the previous section to the multi-robot setting.

A. Basics of multi-robot motion planning

We provide a definition of the multi-robot motion planning (MRMP) problem. We consider the setting of $R \geq 2$ identical robots operating in a shared workspace, and denote by $\mathcal{C}_i \subset [0,1]^d$ the configuration space of robot i, $1 \leq i \leq R$. We define $\mathcal{C}_i^f, \mathcal{C}_i^o \subset \mathcal{C}_i$ to be the free and forbidden spaces, respectively, of robot i. Since the robots are identical it holds that $\mathcal{C}_i^f = \mathcal{C}_j^f$ for all $1 \leq i \leq j \leq R$.

The configuration space of the multi-robot system $\mathbb{C}$, termed *the composite configuration space*, is the Cartesian product of the individual robots' configuration spaces, i.e., $\mathbb{C} = \mathcal{C}_1 \times \ldots \times \mathcal{C}_R$. That is, a composite configuration $Q = (q_1,...,q_R) \in \mathbb{C}$ is an R-tuple of single-robot configurations, where $q_i \in \mathcal{C}_i$. For two distinct robots i, j, we denote by $I_i^j(q_j) \subset \mathcal{C}_i$ the set of configurations of robot i that lead to collision with robot j when j is at configuration q_j. The

composite free space $\mathbb{C}^f \subset \mathbb{C}$ consists of all composite configurations $(q_1,...,q_R)$ such that (i) $q_i \in \mathcal{C}_i^f$ for every $1 \leq i \leq R$, and (ii) $q_i \notin I_i^j(q_j)$ for every $1 \leq i \neq j \leq R$, which ensure that robot-obstacle and robot-robot collisions are avoided, respectively.

Given start and goal positions $x_i^s, x_i^g \in \mathcal{C}_i^f$, respectively, for each robot $1 \leq i \leq R$, define $\vec{x}^s = (x_1^s, \ldots, x_R^s)$ and $\vec{x}^g = (x_1^g, \ldots, x_R^g)$. The MRMP problem, denoted by $\mathbb{M} = (\mathbb{C}^f, \vec{x}^s, \vec{x}^g)$, consists of finding trajectories for the R robots such that the robots begin their motion in $\vec{x}^s$, end at $\vec{x}^g$, and avoid collisions (both with obstacles and with each other) along the way. Formally, the objective is to find a collision-free composite trajectory of the form $\Sigma : [0,1] \to \mathbb{C}^f$, where Σ is an R-tuple $\Sigma = (\sigma_1, ..., \sigma_R)$ of single-robot trajectories $\sigma_i : [0,1] \to \mathcal{C}_i^f$, such that $\Sigma(0) = \vec{x}^s, \Sigma(1) = \vec{x}^g$, and $\Sigma(\tau) \in \mathbb{C}^f$ for all $0 \leq \tau \leq 1$.

In this work we are interested in finding high-quality solutions for the multi-robot problem. We consider as cost criterion the sum of single-robot trajectory lengths, denoted as $\text{cost}(\Sigma) = \sum_{i=1}^R \|\sigma_i\|$. Our analysis can be easily adapted to the case where the cost criterion is the maximum of trajectory lengths, i.e., $\max_{i=1}^R \|\sigma_i\|$.

B. Tensor roadmaps

We provide a formal definition of the tensor roadmap (TR), which is implicitly explored by sampling-based planners such as dRRT [30], dRRT* [31], as well as by search-based methods such as MC-CBS [11] and M* [6].

For every robot i, $1 \leq i \leq R$, let $G_i(\mathcal{X}_i, r_i) = (V_i, E_i)$ be a PRM graph embedded in $\mathcal{C}_i^f$, for some point set $\mathcal{X}_i$ and radius $r_i > 0$ (as defined in Section II-B). The TR, denoted by $\widehat{G}(\vec{\mathcal{X}}, \vec{r}) = (\widehat{V}, \widehat{E})$, is the tensor product of $G_1, \ldots, G_R$. In particular, each vertex of $\widehat{G}(\vec{\mathcal{X}}, \vec{r})$ describes a simultaneous placement of the R robots, and similarly an edge of $\widehat{G}(\vec{\mathcal{X}}, \vec{r})$ describes a simultaneous motion of the robots. Formally,

(i) $\widehat{V} = \{(v_1, \ldots, v_R) : \forall i, v_i \in V_i\}$, and
(ii) for two vertices $W = (w_1, \ldots, w_R), U = (u_1, \ldots, u_R) \in \widehat{V}$, the edge set $\widehat{E}$ contains the edge (W, U) if for all i, $w_i = u_i$ or $(w_i, u_i) \in E_i$.

Note that robots are allowed to stay in place, which differs from prevalent definitions of the tensor product of graphs [36–38]. Notice further that by the definition of G_i, the motion described by each edge in $\widehat{E}$ represents a trajectory for the R robots in which the robot-obstacle collisions are avoided. Next we consider a subgraph of the TR in which also robot-robot collisions are avoided. Given an MRMP problem, $\mathbb{M} = (\mathbb{C}^f, \vec{x^s}, \vec{x^g})$ we will denote as $\widehat{G}_{\mathbb{M}(\vec{\mathcal{X}}, \vec{r})}(x^s, x^g)$ its TR constructed from the PRM graphs of the individual robots' $G_{\mathcal{M}_i}(\mathcal{X}_i, r_i)$, but where *we remove all edges of the TR representing transitions of the robots that are not collision free*. We denote by $d_{\widehat{G}_{\mathbb{M}(\vec{\mathcal{X}}, \vec{r})}}(\vec{x^s}, \vec{x^g})$ the minimal cost of collision-free trajectories from $\vec{x^s}$ to $\vec{x^g}$ in the graph $\widehat{G}_{\mathbb{M}(\vec{\mathcal{X}}, \vec{r})}$.

C. Multi-robot clearance and completeness

In preparation of defining the multi-robot equivalent of (ε, δ)-completeness, we first define clearance for the multi-robot case. Given a trajectory Σ, we define for each robot its forbidden space at time $\tau \in [0,1]$ to be its obstacle space

---

[2]We ignore the roundups for both results as it does not change the asymptotic results.

$\mathcal{C}_i^o$ and the configurations that will lead to collisions with other robots. Formally, $\mathcal{C}_i^o(\tau) = \mathcal{C}_i^o \bigcup_{j\neq i} I_i^j(\sigma_j(\tau))$ is the forbidden space for robot i at time τ. Notice that we define $\mathcal{C}_i^o(\tau)$ only for a given trajectory Σ as it depends on the locations of the other robots.

Definition 5 ($\vec{\delta}$-clearance). Given a trajectory Σ, we say that Σ has $\vec{\delta}$-clearance for $\vec{\delta} = (\delta_1, \ldots, \delta_R)$ if for each robot i, $1 \leq i \leq R$ and at any time $\tau \in [0,1]$, the distance from i to the obstacles and to each robot $j \neq i$ is at least δ_i. Formally, Σ has $\vec{\delta}$-clearance if, for all $1 \leq i \leq R$, $0 \leq \tau \leq 1$, it holds that $\|\sigma_i(\tau) - x\| > \delta_i$, for every $x \in \mathcal{C}_i^o(\tau)$.

Next we define the equivalent of single-robot (ε, δ)-completeness for MRMP:

Definition 6 (Multi-robot $(\varepsilon, \vec{\delta})$-completeness). Given R robots, a stretch parameter $\varepsilon > 0$, a vector of R sample sets $\vec{\mathcal{X}} = (\mathcal{X}_1, \ldots, \mathcal{X}_R)$, and a vector of R connection radii $\vec{r} = (r_1, \ldots, r_R)$, we say that the pair $(\vec{\mathcal{X}}, \vec{r})$ is $(\varepsilon, \vec{\delta})$-complete if for every $\vec{\delta}$-clear $\mathbb{M} = (\mathbb{C}^f, \vec{x^s}, \vec{x^g})$ it holds that
$$d_{\widehat{G}_{\mathbb{M}(\vec{\mathcal{X}}, \vec{r})}}(\vec{x^s}, \vec{x^g}) \leq (1+\varepsilon)\mathrm{OPT}_{\vec{\delta}},$$
where $\mathrm{OPT}_{\vec{\delta}}$ is the minimal cost of a $\vec{\delta}$-clear $\mathbb{M}$ solution.

We are ready to state our main contribution.

Theorem 4 (Sufficient conditions for $(\varepsilon, \vec{\delta})$-completeness). Let $\varepsilon > 0$ be a stretch factor, let $\vec{\delta}$ be a clearance vector $(\delta_1, \ldots, \delta_R)$, and denote $\omega = \frac{\varepsilon}{2(\varepsilon+2)}$. Define the sampling distributions $\vec{\mathcal{X}} = (\mathcal{X}_1, \ldots, \mathcal{X}_R)$ and radii vector $\vec{r} = (r_1, \ldots, r_R)$, as
$$\mathcal{X}_i = \mathcal{X}_{\omega\delta_i, \delta_i}, \quad r_i = \frac{\delta_i(\varepsilon+1)}{(\varepsilon+2)},$$
for every robot $1 \leq i \leq R$. Then $\left(\vec{\mathcal{X}}, \vec{r}\right)$ is $\left(\varepsilon, \vec{\delta}\right)$-complete.

We provide a sketch of the proof. The full proof can be found in the extended version of the paper [33].

Sketch of proof. Let $\Sigma^* = (\sigma_1^*, \ldots, \sigma_R^*)$ be a $\vec{\delta}$-clear solution such that $\mathrm{cost}(\Sigma^*) = \mathrm{OPT}_{\vec{\delta}}$. For every $1 \leq i \leq R$, define $\mathcal{X}_i = \mathcal{X}_{\beta_i, \delta_i}$, and set $\beta_i = \omega\delta_i$. Let $G_i = (V_i, E_i)$ be the PRM graph for robot i using $(\mathcal{X}_i, r_i)$, that is $G_i = G_{\mathcal{M}_i}(\mathcal{X}_i, r_i)$ for $\mathcal{M}_i = (\mathcal{C}_i, x_i^s, x_i^g)$. Let $\widehat{G}$ be the tensor roadmap of $G_1, \ldots, G_R$.

Using Theorem 1 it follows that for every robot i, G_i contains a collision-free path $\bar{\sigma}_i$ (with respect to the obstacles) from x_i^s to x_i^g, such that $\mathrm{cost}(\bar{\sigma}_i) \leq (1+\varepsilon)\|\sigma_i^*\|$, and hence $\mathrm{cost}(\bar{\Sigma}) \leq (1+\varepsilon)\mathrm{OPT}_{\vec{\delta}}$, for $\bar{\Sigma} = (\bar{\sigma}_1, \ldots, \bar{\sigma}_R)$. Although each trajectory $\bar{\sigma}_i$ is collision free with respect to $\mathcal{C}_i^f$, it is not necessarily true that $\bar{\Sigma}$ avoids robot-robot collisions. Nevertheless, we show that we can adjust the robots' timing along the trajectories $\bar{\sigma}_1, \ldots, \bar{\sigma}_R$, to induce a collision-free trajectory over $\widehat{G}$, which we denote by $\widehat{\Sigma} = (\widehat{\sigma}_1, \ldots, \widehat{\sigma}_R)$. As our cost metric is total path length, this timing adjustment does not increase the solution cost.

To do so, we use details from the proof of Theorem 1 (provided in the extended version [33]). In particular, for every robot i, we can pick the trajectory $\bar{\sigma}_i$, which we used above, such that if $Z_i = (z_0^i, \ldots, z_{\ell_i}^i)$ denotes the sequence of vertices of G_i visited along $\bar{\sigma}_i$, and $(\tau_0^i, \ldots, \tau_{\ell_i}^i)$ denote the time of visitation of those vertices, i.e., $z_j^i = \bar{\sigma}_i(\tau_j^i)$, then

the following properties hold for $\rho_i = \frac{\delta_i}{\varepsilon+2}$:
(i') $\|\sigma_i^*(\tau_k^i) - \sigma_i^*(\tau_{k-1}^i)\| \leq \rho_i$, for all $1 \leq k \leq \ell_i$;
(ii') $\|z_k^i - \sigma_i^*(\tau_k^i)\| \leq \beta_i$, for all $0 \leq k \leq \ell_i$;
(iii') $\|z - \sigma_i^*(\tau_k^i)\| \leq \beta_i + \rho_i \leq \delta_i/2$, for all $1 \leq k \leq \ell_i, z \in$ CH$\left(z_{k-1}^i, z_k^i\right)$.

To exploit those properties we define a list $\mathcal{L}$ of triplets of the following form: $\mathcal{L} := \bigcup_{i=1}^R \bigcup_{j=1}^{\ell_i}\{(i, \tau_j^i, z_j^i)\}$. That is, $\mathcal{L}$ contains for every robot $1 \leq i \leq R$, ℓ_i triplets of the form (i, τ_j^i, z_j^i), where $\tau_j^i \in T_i$ is a timestamp, and $z_j^i \in Z_i$ is the corresponding configuration. Additionally, define $\mathcal{L}^o$ to be a permutation of $\mathcal{L}$, where the triplets are ordered according to the timestamp. That is, $\mathcal{L}^o := \{(i_1, \tau_{i_1}, z_{i_1}), \ldots, (i_l, \tau_{i_l}, z_{i_l})\}$, where $l = \sum_{i=1}^R \ell_i$, $(i_j, \tau_{i_j}, z_{i_j}) \in \mathcal{L}$ for every $1 \leq j \leq l$, and $\tau_{i_j} \leq \tau_{i_{j+1}}$ for every $1 \leq j \leq l-1$.

We describe an iterative scheme that uses $\mathcal{L}^o$ for generating a sequence of composite vertices $V_0, V_1, \ldots, V_l \in \widehat{V}$, such that $(V_j, V_{j+1}) \in \widehat{E}$. First, define $V_0 = \vec{x}^s$. Next, given that $V_j = (v_{j_1}, \ldots, v_{j_R})$ has already been defined for some $1 \leq j \leq l-1$, set $V_{j+1} = (v_{(j+1)_1}, \ldots, v_{(j+1)_R})$, where $v_{(j+1)_{i_{j+1}}} := z_{i_{j+1}}$, and $v_{(j+1)_{i'}} = v_{j_{i'}}$ for every $i' \neq i_{j+1}$. Namely, when transitioning from V_j to V_{j+1} all the robots stay put, besides robot i_{j+1} whose timestamp appeared in item $j+1$ of $\mathcal{L}^o$.

For example, consider a two-robot setting with $T_1 = (0, 0.3, 0.5, 0.7, 1)$, $Z_1 = (z_0^1, z_1^1, z_2^1, z_3^1, z_4^1)$, $T_2 = (0, 0.2, 0.4, 0.7, 1)$, $Z_2 = (z_0^2, z_1^2, z_2^2, z_3^2, z_4^2)$. Note that z_0^i is robot i's starting point, and z_4^i is its goal. Then,
$$\mathcal{L} = \{(1, 0.3, z_1^1), (1, 0.5, z_2^1), (1, 0.7, z_3^1), (1, 1, z_4^1),$$
$$(2, 0.2, z_1^2), (2, 0.4, z_2^2), (2, 0.7, z_3^2), (2, 1, z_4^2)\},$$
$$\mathcal{L}^o = \{(2, 0.2, z_1^2), (1, 0.3, z_1^1), (2, 0.4, z_2^2), (1, 0.5, z_2^1),$$
$$(1, 0.7, z_3^1), (2, 0.7, z_3^2), (1, 1, z_4^1), (2, 1, z_4^2)\},$$
yielding the vertices $V_0 = (z_0^1, z_0^2), V_1 = (z_0^1, z_1^2), V_2 = (z_1^1, z_1^2), V_3 = (z_1^1, z_2^2), V_4 = (z_2^1, z_2^2), V_5 = (z_3^1, z_2^2), V_6 = (z_3^1, z_3^2), V_7 = (z_4^1, z_3^2), V_8 = (z_4^1, z_4^2)$.

To complete the proof, we first note that $(V_j, V_{j+1}) \in \widehat{E}$ for every $1 \leq j \leq l-1$. This follows from the values of connection radii $\vec{r}$ we picked, and the fact that $\bar{\sigma}_i$ is obstacle collision-free, guaranteeing that $\{v_i^j, v_{j+1}^i\} \in E_i$ for every robot i, where $(v_1, \ldots, v_R) := V_j, (v_1', \ldots, v_R') := V_{j+1}$.

It remains to prove that the robots do not collide with one another while they move along the path represented by any such edge (V_j, V_{j+1}). First, recall that there is exactly one robot moving for (V_j, V_{j+1}). In particular, this is the robot whose index is i_j, which is the first value of the jth triplet $(i_j, \tau_{i_j}, z_{i_j}) \in \mathcal{L}^o$. That is $v_{i_j} \neq v_{i_j}'$, whereas for any other robot $k \neq i_j$ it holds that $v_k = v_k'$. Note that given two stationary robots $k_1, k_2 \neq i_j$, and assuming that they did not collide along the previous edge (V_{j-1}, V_j), they will not collide with each other for (V_j, V_{j+1}) as well.

Next, we prove that robot i_j does not collide with any stationary robot $k \neq i_j$, while moving from v_{i_j} to v_{i_j}'. By definition of $V_0, \ldots, V_l$, robot k is located at $v_k = z_{j'}^k \in Z_k$ such that $\tau_{j'}^k \leq \tau_{i_j} \leq \tau_{j'+1}^k$, for some $0 \leq j' \leq \ell_k - 1$. Next, recall that $\sigma_k^*, \sigma_{i_j}^*$ are δ_k- and δ_{i_j}-clear, respectively. Thus, it suffices to prove that $\|\sigma_{i_j}^*(\tau_{i_j}) - p\| \leq \delta_{i_j}/2$ for every $p \in \mathrm{CH}\left(v_{i_j}, v_{i_j}'\right)$ and $\|\sigma_k^*(\tau_{i_j}) - z_{j'}^k\| \leq \delta_k/2$.

Indeed, Property (iii') implies that for $p \in \mathrm{CH}\left(v_{i_j}, v'_{i_j}\right)$ we have that $\left\| p - \sigma^*_{i_j}(\tau_{i_j}) \right\| \leq \beta_{i_j} + \rho_{i_j} \leq \delta_{i_j}/2$. Using the triangle inequality and Properties (i') and (ii') we have that

$$\left\| z^k_{j'} - \sigma^*_k(\tau_{i_j}) \right\| \leq \| z^k_{j'} - \sigma^*_k(\tau^k_{j'}) \| + \| \sigma^*_k(\tau^k_{j'}) - \sigma^*_k(\tau_{i_j}) \|$$
$$\leq \beta_k + \rho_k \leq \delta_k/2,$$

which concludes the proof sketch. □

D. Discussion

Theorem 4 implies that if a given MRMP planner is guaranteed to find an optimal collision-free path over a TR, then it is also guaranteed to find a $(1 + \varepsilon)$-approximation of the optimal $\vec{\delta}$-clear trajectory (in the continuous domain), when each `PRM` graph is constructed using the sample set $\mathcal{X}_{\omega\delta_i,\delta_i}$ and radius $r_i = \frac{\delta_i(\varepsilon+1)}{(\varepsilon+2)}$ for each robot $1 \leq i \leq R$.

This statement applies, for instance, to `M*` and `MC-CBS`. The former can be viewed as a refined version of `A*` for searching the TR. The latter implicitly explores the TR by incrementally considering combinations of single-robot trajectories induced by the `PRM` graphs, until a combination that yields a collision-free composite trajectory is found. The `dRRT*` planner implicitly explores the TR via an `RRT`-style random exploration using a secondary sampling procedure which is employed after the `PRM` graphs are constructed. Due to this additional randomization step, `dRRT*` achieves an $(1+\varepsilon)$-approximation only *asymptotically*. Nevertheless, our analysis simplifies the usage of this algorithm by derandomizing the construction of `PRM` graphs used in `dRRT*`.

Finally, we provide an example for the number of samples that should be used according to Theorem 4 within each `PRM` roadmap for specific parameters. In particular, we report in the table below the value $|\mathcal{X}_{\omega\delta_i,\delta_i}|$, for varying values of the stretch parameter ε, dimension d, and clearance vector $(\delta_1, \ldots, \delta_R)$, where $\delta_i = 0.1$ for all robots. While these values are quite large, particularly for higher dimensions, we emphasize that we do not expect our bounds to be tight, as observed in Section IV. This suggests that smaller sample sets are sufficient for $(\varepsilon, \vec{\delta})$-completeness, which we aim to explore in future research (see Section V).

d	$\varepsilon = \infty$	$\varepsilon = 5$	$\varepsilon = 1$	$\varepsilon = 0.5$	$\varepsilon = 0.25$
2	181	313	1201	3281	$1.05 \cdot 10^4$
3	2331	6119	$5.68 \cdot 10^4$	$2.43 \cdot 10^5$	$1.43 \cdot 10^6$
4	$4.93 \cdot 10^4$	$1.49 \cdot 10^5$	$2.83 \cdot 10^6$	$2.19 \cdot 10^7$	$2.21 \cdot 10^8$
5	$9.09 \cdot 10^5$	$4.37 \cdot 10^6$	$1.69 \cdot 10^8$	$2.23 \cdot 10^9$	$3.94 \cdot 10^{10}$
6	$1.89 \cdot 10^7$	$1.5 \cdot 10^8$	$1.18 \cdot 10^{10}$	$2.46 \cdot 10^{11}$	$7.82 \cdot 10^{12}$

IV. EXPERIMENTAL RESULTS

We provide experimental results to support our theoretical findings, focusing on the case of multiple disc robots operating in a planar domain. We study the effect that the stretch parameter ε, which determines the structure of the underlying `PRM` graphs within the tensor product graph $\mathbb{G}$ in Theorem 4, has on the actual solution quality. We observe that the resulting approximation factor is in fact significantly lower than $1 + \varepsilon$. This suggests that our analysis can be further refined to support even sampling distributions with fewer samples (see Section V).

Concerning the design of the experiments, we were faced with two challenges. First, current MRMP algorithms [6, 11, 31] (including our own) are limited in their ability to cope with the large tensor roadmaps required to guarantee path quality according to our analysis; this curbed our ability to go to large numbers of robots in the experiments, and strongly motivates further improving of such algorithms. Secondly, in order to provide meaningful experimental reports, we need yardsticks to compare to; the problem is that optimal MRMP algorithms are not known to be tractable even for the simple case of two unit disc robots moving amid obstacles in the plane, and it is highly non-trivial to calculate optimal solutions when coordination is required. We explain below how we overcame this latter impediment.

A. Scenarios

The scenarios are illustrated in Figure 5. The first scenario, [Left], consists of two robots in an obstacle-free environment. We use this simple example to benchmark our solution against an optimal δ-clear solution using a recent work that provides characterization of optimal trajectories for two disc robots *in the absence of obstacles* [39]. The [Center] scenario uses a more complicated workspace topology, which potentially requires more samples to achieve a near-optimal solution, since multiple straight-line segments are required to approximate every single-robot trajectory. The third scenario, [Right], which consists of seven robots, aims to test our theory for a larger number of robots, where additional coordination is required to achieve a solution.

B. Results

To test our theory on the aforementioned scenarios, we constructed `PRM` graphs using our staggered grid as the sample set, corresponding to different values of the stretch parameter ε and clearance δ (for simplicity, we use the same value of δ across all robots, i.e., $\vec{\delta} := \{\delta, \ldots, \delta\}$). For all the scenarios, we set the value δ to be equal to the *static clearance* μ (see caption of Figure 5). We set the stretch parameter ε to different values in the range $[0.75, \infty)$. We then use `A*`-search for the first two scenarios, and `MC-CBS` for the seven-robot scenario, to obtain the best solution from the resulting tensor roadmap.

The results are reported in Figure 6, where we plot the approximation ratio obtained using the staggered grid $\mathcal{X}_{\omega\delta,\delta}$ set to guarantee an approximation factor of at most $1 + \varepsilon$ (see Theorem 4). The approximation factor that we report represents the ratio between the cost of the best solution obtained from the tensor roadmap, denoted by $\widehat{\Sigma}$, and the optimal δ-clear solution whose cost is denoted by OPT_δ. For the first scenario we obtain the value OPT_δ using [39], as we reported earlier. For the [Center] scenario, OPT_δ is equal to the sum of the shortest δ-clear trajectories for the two individual robots, as one of the robots can move after the other finishes its motion without increasing the overall cost of the solution. For the [Right] scenario, OPT_δ is equal to the sum of the Euclidean distances between each robot's origin and destination, as here as well the robots can move one after the other to obtain an optimal solution.

In all the experiments we obtain an approximation factor that is significantly lower than what our worst-case analysis predicts. For instance, already when setting the stretch parameter to $\varepsilon = 50$ we obtain an approximation factor of at most 1.075. Moreover, for $\varepsilon \leq 1.5$ we obtain approximation
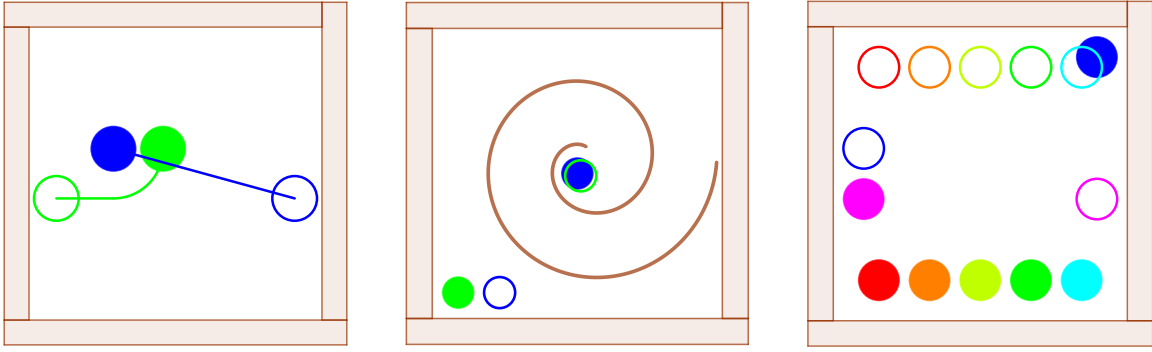
Fig. 5: Test scenarios for multiple disc robots, where an annulus and disc of the same color represents the start and goal positions, respectively, of a robot. [Left] A 2-robot obstacle-free scenario. The optimal trajectories, which were derived in [39], are drawn for each robot. The robots' radius is 0.09 and the static clearance μ is equal to 0.02. The latter value measures the minimum over (i) the inter-robot distances at the initial placement, (ii) the distance of each robot at the initial placement from the obstacles, and (iii,iv) the respective quantities for the target placement. [Center] A 2-robot scenario with a spiral obstacle with robots' radius 0.06 and static clearance $\mu = 0.04$. [Right] A 7-robot scenario with robots' radius 0.08 and the static clearance $\mu = 0.04$.
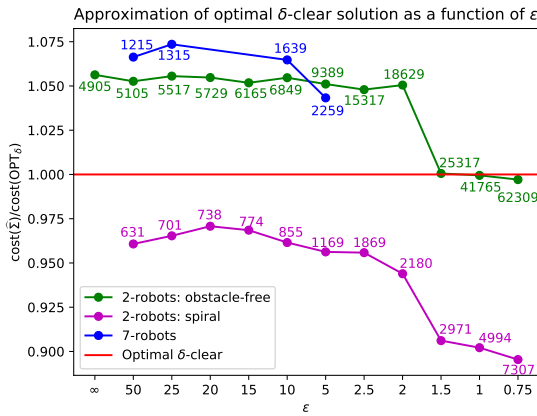

Fig. 6: We report for each of the three scenarios its approximation factors, which are represented by the ratio between the cost of the solution obtained from the tensor roadmap and OPT_δ. Notice that the tensor-roadmap solution is not necessarily δ-clear and thus can be of lower cost than OPT_δ, which explains why two of the plots get approximation factors smaller than 1. Next to the points in each plot is the number of collision-free samples in the PRM graph of an individual robot. Due to the prohibitive running times incurred by MC-CBS on the 7-robot scenario, we report the solution quality for this scenario for four values of ε.

factors below 1 in both two-robot scenarios. This is possible as the solution obtained from the tensor roadmap is not necessarily δ-clear, which allows robots to take shortcuts in proximity to obstacles and each other. The overall trend of the approximation factor is a decrease, where the biggest decrease (at least for the two-robot scenarios) occurs when ε goes below 2, due to the rapid increase in the number of samples in $\mathcal{X}_{\omega\delta,\delta}$. In some cases using a smaller number of samples may yield better solutions, as in the 2-robot spiral scenario for stretch factors $\varepsilon = 50$ and $\varepsilon = 20$. The explanation is that the smaller sample set gets closer to the (approximate) optimal solution by chance. Still, the *worst-case approximation factor* is guaranteed to improve as the size of the staggered grid increases.

V. DISCUSSION AND FUTURE WORK

We developed sufficient theoretical conditions for finite-sample near-optimality of the tensor roadmap, which is an underlying structure in several sampling-based algorithms for MRMP planning. We also presented a new sampling-scheme, termed the staggered grid, for near-optimal motion planing for individual robots, which requires fewer samples than previous work.

Our work raises interesting questions for further investigation both in practice and theory. The scalability issues we encountered when testing our theoretical finding on MC-CBS—a continuous extension of a state-of-the-art method for MAPF—motivate the study of more effective methods for exploring tensor roadmaps introduced by large PRM graphs. On the positive side, the scenarios that we did manage to solve suggest that near-optimality can be achieved with smaller sample sets than our theory prescribes. This motivates the development of even more compact sampling-distributions for the single-robot case, and refining our proof technique for the multi-robot case (Theorem 4).

ACKNOWLEDGMENTS

REFERENCES

[1] K. Solovey and D. Halperin, "On the hardness of unlabeled multi-robot motion planning," *International Journal of Robotic Research*, vol. 35, no. 14, pp. 1750–1759, 2016.

[2] P. G. Spirakis and C.-K. Yap, "Strong NP-hardness of moving many discs," *Information Processing Letters*, vol. 19, no. 1, pp. 55–59, 1984.

[3] J. E. Hopcroft, J. T. Schwartz, and M. Sharir, "On the complexity of motion planning for multiple independent objects; PSPACE-hardness of the "Warehouseman's problem"," *International Journal of Robotics Research*, vol. 3, no. 4, pp. 76–88, 1984.

[4] J. K. Johnson, "On the relationship between dynamics and complexity in multi-agent collision avoidance," *Autonomous Robots*, vol. 42, no. 7, pp. 1389–1404, 2018.

[5] S. D. Han and J. Yu, "Effective heuristics for multi-robot path planning in warehouse environments," in *2019 International Symposium on Multi-Robot and Multi-Agent Systems (MRS)*. IEEE, 2019, pp. 10–12.

[6] G. Wagner and H. Choset, "Subdimensional expansion for multirobot path planning," *Artificial Intelligence*, vol. 219, pp. 1–24, 2015.

[7] G. Sharon, R. Stern, A. Felner, and N. R. Sturtevant, "Conflict-based search for optimal multi-agent pathfinding," *Artificial Intelligence*, vol. 219, pp. 40–66, 2015.

[8] H. Ma, W. Hönig, T. K. S. Kumar, N. Ayanian, and S. Koenig, "Lifelong path planning with kinematic constraints for multi-agent pickup and delivery," in *Conference on Artificial Intelligence,, AAAI*.

[9] S. Choudhury, K. Solovey, M. J. Kochenderfer, and M. Pavone, "Efficient large-scale multi-drone delivery using transit networks," in *International Conference on Robotics and Automation (ICRA)*, 2020, pp. 4543–4550.

[10] W. Hönig, T. K. S. Kumar, L. Cohen, H. Ma, H. Xu, N. Ayanian, and S. Koenig, "Summary: Multi-agent path finding with kinematic constraints," in *International Joint Conference on Artificial Intelligence*, 2017, pp. 4869–4873.

[11] J. Li, P. Surynek, A. Felner, H. Ma, T. K. S. Kumar, and S. Koenig, "Multi-agent path finding for large agents," in *Conference on Artificial Intelligence AAAI*, 2019, pp. 7627–7634.

[12] I. Solis, R. Sandstrom, J. Motes, and N. M. Amato, "Roadmap-optimal multi-robot motion planning using conflict-based search," *CoRR*, vol. abs/1909.13352, 2019.

[13] A. Adler, M. de Berg, D. Halperin, and K. Solovey, "Efficient multi-robot motion planning for unlabeled discs in simple polygons," *IEEE Trans. Automation Science and Engineering*, vol. 12, no. 4, pp. 1309–1317, 2015.

[14] I. Solomon and D. Halperin, "Motion planning for multiple unit-ball robots in $\mathbb{R}^d$," in *Workshop on the Algorithmic Foundations of Robotics, WAFR*, 2018, pp. 799–816.

[15] M. Turpin, N. Michael, and V. Kumar, "Trajectory planning and assignment in multirobot systems," in *Workshop on the Algorithmic Foundations of Robotics (WAFR), MIT, Cambridge, Massachusetts, USA*, 2012, pp. 175–190.

[16] K. Solovey, J. Yu, O. Zamir, and D. Halperin, "Motion planning for unlabeled discs with optimality guarantees," in *Robotics: Science and Systems*, 2015.

[17] L. E. Kavraki, P. Svestka, J. . Latombe, and M. H. Overmars, "Probabilistic roadmaps for path planning in high-dimensional configuration spaces," *IEEE Transactions on Robotics and Automation*, vol. 12, no. 4, pp. 566–580, 1996.

[18] L. E. Kavraki, M. N. Kolountzakis, and J. . Latombe, "Analysis of probabilistic roadmaps for path planning," *IEEE Transactions on Robotics and Automation*, vol. 14, no. 1, pp. 166–171, 1998.

[19] J. J. Kuffner and S. M. LaValle, "RRT-Connect: An efficient approach to single-query path planning," in *IEEE International Conference on Robotics and Automation (ICRA)*, 2000, pp. 995–1001.

[20] M. Kleinbort, K. Solovey, Z. Littlefield, K. E. Bekris, and D. Halperin, "Probabilistic completeness of RRT for geometric and kinodynamic planning with forward propagation," *IEEE Robotics Autom. Lett.*, 2018.

[21] L. Janson, E. Schmerling, A. Clark, and M. Pavone, "Fast marching tree: A fast marching sampling-based method for optimal motion planning in many dimensions," *The International Journal of Robotics Research*, vol. 34, no. 7, pp. 883–921, 2015.

[22] S. Karaman and E. Frazzoli, "Sampling-based algorithms for optimal motion planning," *International Journal of Robotics Research*, vol. 30, no. 7, pp. 846–894, 2011.

[23] K. Solovey, L. Janson, E. Schmerling, E. Frazzoli, and M. Pavone, "Revisiting the asymptotic optimality of RRT*," in *IEEE International Conference on Robotics and Automation (ICRA)*, 2020, pp. 2189–2195.

[24] K. Hauser and Y. Zhou, "Asymptotically optimal planning by feasible kinodynamic planning in a state-cost space," *IEEE Trans. Robotics*, vol. 32, no. 6, pp. 1431–1443, 2016.

[25] M. Kleinbort, E. Granados, K. Solovey, R. Bonalli, K. E. Bekris, and D. Halperin, "Refined analysis of asymptotically-optimal kinodynamic planning in the state-cost space," in *IEEE International Conference on Robotics and Automation (ICRA)*, 2020, pp. 6344–6350.

[26] G. Sánchez-Ante and J. Latombe, "Using a PRM planner to compare centralized and decoupled planning for multi-robot systems," in *IEEE International Conference on Robotics and Automation (ICRA)*, 2002, pp. 2112–2119.

[27] P. Švestka and M. H. Overmars, "Coordinated path planning for multiple robots," *Robotics and Autonomous Systems*, vol. 23, no. 3, pp. 125–152, 1998.

[28] K. Solovey and D. Halperin, "k-Color multi-robot motion planning," *International Journal of Robotic Research*, vol. 33, no. 1, pp. 82–97, 2014.

[29] A. Krontiris, R. Shome, A. Dobson, A. Kimmel, and K. E. Bekris, "Rearranging similar objects with a manipulator using pebble graphs," in *IEEE-RAS International Conference on Humanoid Robots, Humanoids*, 2014, pp. 1081–1087.

[30] K. Solovey, O. Salzman, and D. Halperin, "Finding a needle in an exponential haystack: Discrete RRT for exploration of implicit roadmaps in multi-robot motion planning," *The International Journal of Robotics Research*, vol. 35, no. 5, pp. 501–513, 2016.

[31] R. Shome, K. Solovey, A. Dobson, D. Halperin, and K. E. Bekris, "dRRT*: Scalable and informed asymptotically-optimal multi-robot motion planning," *Auton. Robots*, vol. 44, no. 3-4, pp. 443–467, 2020.

[32] M. Tsao, K. Solovey, and M. Pavone, "Sample complexity of probabilistic roadmaps via epsilon-nets," in *IEEE International Conference on Robotics and Automation (ICRA)*, 2020.

[33] D. Dayan, K. Solovey, M. Pavone, and D. Halperin, "Near-optimal multi-robot motion planning with finite sampling," *CoRR*, 2020, forthcoming.

[34] K. Solovey and M. Kleinbort, "The critical radius in sampling-based motion planning," *International Journal of Robotics Research*, vol. 39, no. 2-3, pp. 266–285, 2020.

[35] R. Herbrich, *Learning kernel classifiers: theory and algorithms.* MIT press, 2001.

[36] R. Hammack, W. Imrich, and S. Klavzar, *Handbook of Product Graphs, Second Edition*, 2nd ed. USA: CRC Press, Inc., 2011.

[37] R. Balakrishnan and P. Paulraja, "Hamilton cycles in tensor product of graphs," *Discrete Mathematics*, vol. 186, no. 1, pp. 1 – 13, 1998.

[38] Shitov, "Counterexamples to Hedetniemi's conjecture," *Annals of Mathematics*, vol. 190, no. 2, p. 663, 2019.

[39] D. G. Kirkpatrick and P. Liu, "Characterizing minimum-length coordinated motions for two discs," *CoRR*, vol. abs/1607.04005, 2016.